Published in final edited form as:

Nature. 2015 February 26; 518(7540): 560–564. doi:10.1038/nature14234.

N^6-methyladenosine-dependent RNA structural switches regulate RNA-protein interactions

Nian Liu[1], **Qing Dai**[1], **Guanqun Zheng**[2], **Chuan He**[1,3], **Marc Parisien**[2,4,*], and **Tao Pan**[2,3,*]

[1]Department of Chemistry, The University of Chicago, Chicago, IL 60637, USA.

[2]Department of Biochemistry and Molecular Biology, The University of Chicago, Chicago, IL 60637, USA.

[3]Institute for Biophysical Dynamics, The University of Chicago, Chicago, IL 60637, USA.

Abstract

RNA-binding proteins control many aspects of cellular biology through binding single-stranded RNA binding motifs (RBM)[1-3]. However, RBMs can be buried within their local RNA structures[4-7], thus inhibiting RNA-protein interactions. *N*^{6}-methyladenosine (m^{6}A), the most abundant and dynamic internal modification in eukaryotic messenger RNA[8-19], can be selectively recognized by the YTHDF2 protein to affect the stability of cytoplasmic mRNAs[15], but how m^{6}A achieves wide-ranging physiological significance needs further exploration. Here we show that m^{6}A controls the RNA-structure-dependent accessibility of RBMs to affect RNA-protein interactions for biological regulation; we term this mechanism "m^{6}A-switch". We found that m^{6}A alters the local structure in mRNA and long non-coding RNA (lncRNA) to facilitate binding of heterogeneous nuclear ribonucleoprotein C (hnRNP C), an abundant nuclear RNA-binding protein responsible for pre-mRNA processing[20-24]. Combining PAR-CLIP and m^{6}A/MeRIP approaches enabled us to identify 39,060 m^{6}A-switches among hnRNP C binding sites; and global m^{6}A reduction decreased hnRNP C binding at 2,798 high confidence m^{6}A-switches. We determined that these m^{6}A-switch-regulated hnRNP C binding activities affect the abundance as well as alternative splicing of target mRNAs, demonstrating the regulatory role of m^{6}A-switches on gene expression and RNA maturation. Our results illustrate how RNA-binding proteins gain regulated access to their RBMs through m^{6}A-dependent RNA structural remodeling, and provide a new direction for investigating RNA-modification-coded cellular biology.

Post-transcriptional m^{6}A RNA modification is indispensable for cell viability and development, yet its functional mechanisms are still poorly understood[8-19]. We recently identified one m^{6}A site in a hairpin-stem on the human lncRNA MALAT1 (Metastasis

---

*Correspondence: marc.parisien@mcgill.ca, taopan@uchicago.edu.
[4]Present address: Faculty of Dentistry, McGill University, Montreal, Quebec H3A 0G1, Canada

Author contributions N.L., G.Z., M.P. designed and performed experiments, and analyzed data. Q.D. synthesized all RNA oligos. N.L., M.P. and T.P. conceived the project. N.L. and T.P. wrote the paper with input from C.H. and M.P.

Author Information All RNA sequencing data were deposited in the Gene Expression Omnibus (http://www.ncbi.nlm.nih.gov/geo) under accession number GSE56010.

The authors declare no competing financial interests.

Associated Lung Adenocarcinoma Transcript)[25] (Extended Data Fig. 1a). Native gel shift assay indicated that this m^{6}A residue increases the interaction of this RNA hairpin with proteins in the HeLa nuclear extract (Fig. 1a). RNA pull down assays identified heterogeneous nuclear ribonucleoprotein C1/C2 (hnRNP C) as the protein component of the nuclear extract that binds more strongly with the m^{6}A-modified hairpin (Fig. 1b and Extended Data Fig. 1b, c). Stronger binding of the methylated hairpin was validated qualitatively by UV crosslinking and quantitatively (~8-fold increase) by filter-binding using recombinant hnRNP C1 protein (Fig. 1c and Extended Data Fig. 1d).

The hnRNP C protein belongs to the large family of ubiquitously expressed heterogeneous nuclear ribonucleoproteins which bind nascent RNA transcripts to affect premRNA stability, splicing, export and translation[20-24]. hnRNP C preferably binds single-stranded U-tracts (5 or more contiguous uridines)[20,23-24,26-27]. In the MALAT1 hairpin, hnRNP C binds a U_5-tract which is half buried in the hairpin-stem opposing the A/m^{6}A2,577 site (Extended Data Fig. 1a, e).

Since m^{6}A residues within RNA stems can destabilize the thermo-stability of model RNA duplexes[28], we hypothesized that the m^{6}A2,577 residue destabilizes this MALAT1 hairpin-stem to make its opposing U-tract more single-stranded or accessible, thus enhancing its interaction with hnRNP C. We performed several experiments to validate this hypothesis. First, according to the RNA structural probing assays, the m^{6}A-modified hairpin showed significantly increased nuclease S1 digestion (single-stranded specific) at the GAC (A= m^{6}A) motif as well as markedly decreased RNase V1 digestion (double-stranded/stacking specific) at the U-tract opposing the GAC motif (Fig. 1d). The m^{6}A residue markedly destabilized the stacking properties of the region centered around the U-residue that pairs with A/m^{6}A2,577 (Extended data Fig. 1f-g), which was also supported by the increased reactivity between CMCT and the U-tract bases in the presence of m^{6}A (Extended Data Fig. 1h). Second, the A2,577-to-U mutation increased hnRNP C pull down amount from nuclear extract, whereas U-to-C mutations in the U-tract significantly reduced hnRNP C pull down amount regardless of m^{6}A modification (Fig. 1e). Third, the A2,577-to-U mutation increased the accessibility of U-tract and enhanced hnRNP C binding by ~4-fold (Extended data Fig. 2a-c). Binding results with 4 other mutated A/m^{6}A oligos also supported the U-tract with increased accessibility alone being sufficient to enhance hnRNP C binding (Extended data Fig. 2d). Fourth, RNA terminal truncation followed by hnRNP C binding identified two pairs of truncated hairpins with highly accessible U-tracts, which improved hnRNP C binding significantly but independent of the m^{6}A modification (Extended data Fig. 2ei). All these results confirmed that m^{6}A modification can alter its local RNA structure and enhance the accessibility of its base-paired residues or nearby regions to modulate protein binding (Fig. 1f). We term this mechanism that regulates RNA-protein interactions through m^{6}A-dependent RNA structural remodeling as “m^{6}A-switch”.

We performed two experiments to determine the global effect of m^{6}A-switches on hnRNP C binding. First, *in vivo* cross-linking followed by immunoprecipitation and two-dimensional thin-layer chromatography (CLIP-2dTLC) showed that the m^{6}A/A ratio of the hnRNP C bound RNA regions had ~6-fold higher m^{6}A level than the hnRNP C bound intact RNA, and ~3-fold higher m^{6}A level than the flow through RNA (Fig. 2a and Extended Data Fig.

3a). Second, the hnRNP C bound RNA regions had much higher anti-m^{6}A pull down yield (4.3%) than the polyA$^+$ RNA samples (0.5%) using the previously established m^{6}A antibody[13,14] (Fig. 2b). These results indicate widespread presence of m^{6}A residues in the vicinity of hnRNP C binding sites.

To map the m^{6}A sites around hnRNP C binding sites, we performed Photoactivatable-Ribonucleoside-Enhanced Crosslinking and Immunoprecipitation (PAR-CLIP)[29] to isolate all hnRNP C bound RNA regions (Input control) followed by anti-m^{6}A immunoprecipitation (MeRIP)[13,14] to enrich m^{6}A-containing hnRNP C bound RNA regions (IP). Both the Input control and IP samples from two biological replicates were sent for RNA-seq (Fig. 2c and Extended data Fig. 3b, c). This approach, termed PARCLIP-MeRIP, identified transcriptome-wide the m^{6}A proximal hnRNP C binding site, such as the enriched peak around the MALAT1-2,577 site (Fig. 2d). Remarkably, hnRNP C PARCLIP-MeRIP peaks harbored two consensus motifs, the hnRNP C RBM (U-tracts) and the m^{6}A consensus motif GRACH (a subset of RRACH[13,14]) (Fig. 2e). Both motifs were located mostly within 50 residues, suggesting transcriptome-wide RRACH-U-tract coupling events within the hnRNP C binding sites (Extended Data Fig. 4a, b). About 62% of all RRACH-U-tracts coupling events within hnRNP C binding sites are enriched at the RRACH motif (Fig. 2f). Our PARCLIP-MeRIP approach identified a total of 39,060 hnRNP C m^{6}A-switches which corresponded to m^{6}A-modified RRACH-U-tracts coupling events at FDR ≤5% (Extended Data Fig. 4c). These switches account for ~7% of 592,477 hnRNP C binding sites identified by PAR-CLIP. The majority (87%) of m^{6}A-switches occur within introns (Extended Data Fig. 4d, e), consistent with the literature that hnRNP C is nuclear localized and primarily binds nascent transcripts[20,23]. We validated two intronic m^{6}A-switches in hairpin structures where m^{6}A residues increase the U-tract accessibility, and enhance hnRNP C binding by ~3-4 fold (Fig. 2g, h and Extended data Fig. 5).

To assess the effect of global m^{6}A reduction on RNA-hnRNP C interactions, we performed hnRNP C PAR-CLIP experiments in *METTL3* and *METTL14* knockdown (KD) cells (Extended Data Fig. 6a). We identified 16,582 coupling events with decreased U-tracts-hnRNP C interactions upon *METTL3* KD and *METTL14* KD (*METTL3/L14* KD) with significant overlaps at FDR ≤5% (Fig. 3a and Extended Data Fig. 6b, c). In total, 2,798 m^{6}A-switches identified by PARCLIP-MeRIP experiments showed decreased hnRNP C binding upon *METTL3/L14* KD (Fig. 3b) and this number is likely under-estimated due to the fact that *METTL3/L14* KD reduces the global m^{6}A level by only ~30-40% [11,12]. These sites composed the high confidence m^{6}A-switches (HCS) that were used for subsequent analysis.

HCS m^{6}A-switches are enriched in the introns of coding and non-coding RNAs (Fig. 3c and Extended Data Fig. 6d). Exonic m^{6}A-switches are enriched at the middle of exons while intronic m^{6}A-switches are slightly enriched near the 5′ end (Fig. 3d). m^{6}A-switches within coding RNAs tend to locate at very long exons (Extended Data Fig. 6e) and are enriched near the stop codon and in the 3′UTR (Fig. 3e), consistent with the known topology of human m^{6}A methylome in mRNAs[13,14]. Transcriptome-wide RNA structural mapping[4-7] on HCS m^{6}A-switches yielded consistent structural patterns with our three demonstrated m^{6}A-switch hairpins (Fig. 3f). The “RR” residues in the RRACH motif and the 3’ U-tract residues

show increased structural dynamics in the presence of m^{6}A. Besides, m^{6}A-switches prefer short RRACH-U-tract inter-motif distances, are not involved in the previously reported inter-U-tract motif patterns and are conserved across species (Fig. 3g and Extended Data Fig. 6f-i).

To reveal the function of m^{6}A-switches on RNA biology, we performed polyA$^+$ RNA-seq from *HNRNPC*, *METTL3, METTL14* KD and control cells (Extended Data Fig. 7a). *METTL3/L14* KD, which has been shown to decrease hnRNP C binding transcriptome-wide, co-regulated the expression of 5,251 genes with *HNRNPC* KD. In comparison, *METTL3/L14* KD co-regulated only 24 genes with KD of another mRNA binding protein hnRNP U (Extended Data Fig. 7b), which was not enriched in our m^{6}A-hairpin pull down (Fig. 1b). Approximately 45% of 1,815 HCS m^{6}A-switch-containing genes were co-regulated by *HNRNPC*, *METTL3/L14* KD, indicating that m^{6}A-switch-regulated hnRNP C binding affects the abundance of target mRNAs. Gene Ontology (GO) analysis suggests that m^{6}A-switch-regulated gene expression may influence “cell proliferation” and other biological processes (Extended data Fig. 7c). The m^{6}A-switch-regulated expression of genes within these GO categories was validated by qPCR (Fig. 4a and Extended Data Fig. 7d-g). We also found that *HNRNPC*, *METTL3* and *METTL14* KD decreased cell proliferation rate to similar extents (Extended Data Fig. 7h).

Besides the mRNA abundance level changes, we also observed splicing pattern changes within HCS m^{6}A-switch-containing transcripts by DEXSeq[30]. *HNRNPC* KD co-up/down-regulated 131/127 exons with *METTL3* KD and 130/115 exons with *METTL14* KD. These co-regulated exons occur more frequently in the vicinity of m^{6}A-switches than those non-co-regulated exons (Fig. 4b, c), indicating that m^{6}A-switches tend to regulate splicing events at nearby exons. We investigated the splicing pattern at two exons with neighboring m^{6}A-switches: the PARCLIP-MeRIP and *METTL3/L14* KD data confirmed the hnRNP C binding signature at the m^{6}A-switch site neighboring these exons; and *HNRNPC*, *METTL3/L14* KD co-inhibited exon inclusion in both cases (Fig. 4d-f and Extended Data Fig. 8b-f). Besides, we identified 155 genes with multiple m^{6}A-switches exhibiting more than two splice variants, and 221 m^{6}A-switch-containing genes with differentially expressed splice variants in *HNRNPC* and *METTL3/L14* KD samples. Further analysis suggested m^{6}A-switches’ effect on intron exclusion (Extended Data Fig. 8g). Consistent with previous reports about the splicing regulation by both hnRNP C and m^{6}A[13,19,20,23], our results indicate that m^{6}A functions as RNA structure remodeler to affect mRNA maturation through interfering with post-transcriptional regulator binding activities.

In summary, we demonstrated that post-transcriptional m^{6}A modifications could modulate the structure of coding and non-coding RNAs to regulate RNA-hnRNP C interactions, thus influencing gene expression and maturation in the nucleus. It is possible that m^{6}A could also recruit additional accessory factors, such as the YTH domain proteins that can directly recognize m^{6}A as previously reported[15], to destabilize the RNA structure and facilitate hnRNP C binding. Besides hnRNP C, m^{6}A-switches may regulate the function of many other RNA-binding proteins through modulating the RNA-structure-dependent accessibility of their RBMs. Our work indicates widespread m^{6}A-induced mRNA and lncRNA structural remodeling that affect RNA-protein interactions for biological regulation.

Methods

Mammalian cell culture, siRNA knockdown and Western blot

Human cervical cancer cell line HeLa (CCL-2) and embryonic kidney cell line HEK293T (CRL-11268) were obtained from American Type Culture Collection (ATCC) and were cultured under standard conditions. Control siRNA (1027281, Qiagen), METTL3 siRNA (SI04317096, Qiagen), METTL14 siRNA (SI04317096, Qiagen) or HNRNPC siRNA (10620318, Invitrogen) were transfected into HEK293T cells at a concentration of 40 nM using lipofectamine RNAiMAX (Invitrogen) according to the manufacturer's instructions. Cells were collected 48 hours after the transfection, shock-frozen in liquid nitrogen, and stored at -80 °C for further studies. Western blot analysis using METTL3- (HPA038002, Sigma), METTL14- (HPA038002, Sigma), hnRNP C- (sc-32308, Santa Cruz), GAPDH- (A00192-40, Genescript) specific antibodies was performed under standard procedures. Blotting membranes were stained by ECL-prime (RPN2232, GE Healthcare) and visualized by a digital imaging system (G: BOX, SYNGENE). All synthetic oligos were synthesized by Q.D.

Gel shift, RNA pull down and filter binding assay

HeLa nuclear extracts were isolated using the NE-PER Nuclear and Cytoplasmic Extraction Reagents (78833, Thermo Scientific) according to the manufacturer's instructions. The purified radioactively-labeled RNA oligos were refolded by heating at 90 °C for 1 min, then 30 °C for 5 min. 3 μl HeLa nuclear extract and 6 μl refolded RNA were incubated at room temperature (RT) for 30 min and then at 4 °C for 2 hrs. Each sample was mixed with 1 μl 50% glycerol, separated on the 8% native 1x TBE gel, and visualized by phosphorimaging using the Personal Molecular Imager (Bio-Rad).

The *in vitro* pull down assay was performed as described[13]. The eluted protein samples were separated on 4-12% polyacrylamide Bis-Tris gels (NP0321BOX, Invitrogen) and stained with SYPRO-Ruby (S12000, Invitrogen) according to the manufacturer's instructions. Protein in gel slices or the entire pulled down protein samples were digested with trypsin and identified using LC-MS/MS by the Donald Danforth Plant Science Center (Washington University, St. Louis. MO). The RNA oligos used in Fig. 1f: 2,577-U: 5'-AACUUAAUGUUUUUGCAUUGGUCUUUGAGUUA-Biotin; CC-2,577-A: 5'-AACUUAAUGUCCUUGCAUUGGACUUUGAGUUA-Biotin; CC-2,577-m^6A: 5'-AACUUAAUGUCCUUGCAUUGGm^6ACUUUGAGUUA-Biotin.

The full-length hnRNP C1 protein were purified and *in vitro* UV crosslinking assay were performed as previously described[23]. Filter-binding assays were performed as previously described[24].

CLIP-2dTLC

HEK293T cells at 70-80% confluency were UV irradiated with 400 mJ/cm^2 at 254 nm, and harvested by centrifuging at 4,000 rpm for 3 min at 4 °C (with centrifugation rotor #75003524, Fisher scientific). The pellet of cross-linked cells were resuspended in 1 ml lysis buffer (1x PBS, 0.1% SDS, 1% Nonidet P-40, 0.5% Sodium Deoxycholate, protease

inhibitor cocktail and RNase inhibitor) and incubated on ice for 4 hrs. Cell lysate was isolated by centrifuging at 3,000 rpm for 5 min and pre-blocked with 50 μl protein A beads in 300 μl lysis buffer. Another 50 μl protein A beads (Invitrogen) were incubated with 8 μg corresponding antibodies for 4 h at room temperature, and then mixed with the pre-blocked cell lysate at 4 °C overnight. The beads were washed 3 times with 1 ml wash buffer (20 mM Tris-HCl pH 7.4, 10 mM $MgCl_2$, 0.2% Tween-20), 3 times with 1 ml high salt buffer (5x PBS, 0.1% SDS, 1% Nonidet P-40, 0.5% Sodium Deoxycholate), and 3 times with 1 ml wash buffer. The beads were resuspended in 1 ml wash buffer, and divided into 2x 500 μl in two separate tubes. One tube was incubated with 200 μl RNase T1/A mixture at room temperature for 1 h. The other tube was incubated with 200 μl nuclease-free water at room temperature for 1 h. The beads were washed 3 times with 1 ml high salt buffer, and 3 times with 1 ml wash buffer. Crosslinked RNA was eluted from beads by incubating with 200 μl RNA elution buffer (100 mM Tris-HCl pH 7.4, 10 mM EDTA, 1% SDS) containing 2 mg/ml proteinase K at 50 °C for 30 min followed by phenol/chloroform extraction. The RNA pellet was dissolved in 7 μl nuclease-free water containing 1 μl RNase T1 (200 U), heated at 65 °C for 2 min, and incubated at 37 °C for 30 min. The T1-digested RNA fragments were labeled upon adding 2 μl T4 PNK mix (4.5 U/μl T4 PNK, 600 Ci/mmol [γ-^{32}P] ATP, 5x PNK buffer) and incubation at 37 °C for 30 min. Unreacted [γ-^{32}P] ATP was removed using Illustra MicroSpin G-25 columns. The eluted RNA was digested with 1 μl (1U/ μl) nuclease P1 at 37 °C for 1 h. Samples were spotted on cellulose TLC plate and 2D TLC was run as described[25] using isobutyric acid: 0.5 M NH_4OH (5:3, v/v) as the first dimension and isopropanol:HCl:water (70:15:15, v/v/v) as the second dimension.

RNA structural probing and RNA terminal truncation

The synthetic RNA oligos were 5′ end-labeled with γ-^{32}P-ATP by T4 PNK (70031, Affymetrix), gel purified, and re-folded. Structural probing assay with RNase T1, nuclease S1 and RNase V1 was performed as previously described[25]. Note: 3′-end-labeled HNRNPH1 oligos were used for RNA structural probing assay in Fig. 2g.

CMCT RNA structural probing assay was performed as reported[32]. RNA refolding: 3 pmole RNA was annealed in 50 mM potassium borate (pH 8) by heating at 90 °C for 1.5 min then incubation at RT for 3 min.

RNA terminal truncation assay was carried out as previously reported[33]. RNA samples were first alkaline-hydrolyzed as in the RNA structural probing assay, and then incubated with hnRNP C1 protein in the same conditions as in the filter binding assay. The RNA-Protein complexes were then loaded onto filter papers and washed twice with chilled binding buffer. Air dry filters and RNA samples were then extracted from the filters and loaded onto denaturing gel as in the RNA structural probing assay.

PARCLIP and PARCLIP-MeRIP

PAR-CLIP procedures were performed as previously reported[29] with the following modification. HEK293T cells in 15 cm plates treated following normal PAR-CLIP procedures were lysed and digested with a combination of RNase I (Ambion, AM2295, 15 μl 1/50 diluted with H_2O) and Turbo DNases (2 μl) for 3 mins at 37 °C, shaking at 1,100

rpm. The lysate was then immediately cleared by spinning at 14,000 rpm, 4 °C for 30 min, and placed on ice for further use. hnRNP C binding sites were identified by PARalyzer v1.1[34] with default settings.

PARCLIP-MeRIP experiment applied m^{6}A-antibody immunoprecipitation[13,14,35] to the hnRNP C PAR-CLIP RNA samples. The hnRNP C PAR-CLIP RNA sample was incubated with m^{6}A-specific antibody (202003, SYSY), RNase inhibitor (80 units, Sigma-Aldrich), human placental RNase inhibitor (NEB) in 200 μl 1x IP buffer (50 mM Tris-HCl pH 7.4, 750 mM NaCl and 0.5% (vol/vol) Igepal CA-630) at 4 °C for 2 hours under gentle shaking conditions. For each PARCLIP-MeRIP experiment, 20 μl protein-A beads (Invitrogen) were washed twice with 1 ml 1x IP buffer, blocked with 2 hours incubation with 100 μl 1× IP buffer supplemented with BSA (0.5 mg/ml), RNasin and Human placental RNase inhibitor, and then washed twice with 100 μl 1x IP buffer. The pre-blocked protein-A beads were then combined with the prepared immuno-reaction mixture and incubated at 4 °C for 2 hours, followed by three washes with 100 μl 1× IP buffer. After that, the RNA was eluted by 1 hour incubation with 20 μl elution buffer (1× IP buffer and 6.7 mM m^{6}A, Sigma-Aldrich) under gentle shaking conditions, and purified by ethanol precipitation. The purified RNA sample (IP) as well as the input PAR-CLIP RNA sample (Input control) were used for library construction by Truseq small RNA sample preparation kit (Illumina).

Libraries were prepared using TruSeq Small RNA Sample Preparation Kit (RS-200-0012, Illumina) according to the manufacturer's instructions, and then sequenced by Illumina Hiseq2000 with single end 50-bp read length. The control and IP samples from PARCLIP MeRIP experiments (same case for the control and KD samples from *METTL* KD experiments) were sequenced together in one flowcell on two lanes, and the reads from two lanes of each sample were combined for remaining analysis. The raw seq data was trimmed using the Trimmomatic computer program version 0.30[36] to remove adaptor sequences, and mapped to the Human genome version hg19 by Bowtie 1.0.0[37] without any gaps and allowed for at most two mismatches.

Detection of PARCLIP-MeRIP peaks and differential PAR-CLIP peaks

The raw read counts of the biological replicates confirmed the reproducibility between replicates (Extended Data Fig. 9), and replicates were combined for subsequent analysis. For each genomic site, we calculated the average read counts within an 11-nt window centered at that site, as the normalized read counts for that site. This normalization smoothed the raw mapping curves, and facilitated identification of peaks within each mapping cluster. To correct for changes in sequencing depth or expression levels between samples, we then normalized the read counts at each genomic site to the total number of read counts on the respective gene. The above defined double-normalization procedures enabled precise identification of changes in the mapping reads at specific genomic locations by directly comparing the normalized read counts between samples. No read counts in the intergenic region were compared between samples, because the transcription boundaries are not defined at this region and the intergenic read counts cannot be normalized to correct changes for transcript expression.

Detection of PARCLIP-MeRIP peaks involves comparing the read counts of the IP sample with that of the control (Ctrl) sample as follows: (i) we identified all peaks within hnRNP C binding sites in the IP sample; (ii) we performed transcriptome-wide scanning to compare read counts of each identified peak in (i) with read counts at same genomic locations in the Ctrl sample to calculate the fold change score, score = $\log_2 (H_{IP}/H_{Ctrl})$. The score threshold was set to be 1, corresponding to a twofold increase compared with control.

Detection of decreased hnRNP C binding sites involved comparing hnRNP C occupancies in the *METTL* KD (KD) sample with that in control as follows: (i) we identified all peaks within hnRNP C binding sites in the *METTL* KD sample; (ii) we performed transcriptome-wide scanning to compare read counts of each identified peak in (i) with read counts at the same genomic locations in control to calculate the fold change score, score = $\log_2 (H_{KD}/H_{Ctrl})$. The score threshold was set to be -1, corresponding to a twofold decrease compared with control.

Identification of enriched motifs and hnRNP C m^{6}A-switches

To identify enriched motifs, we first sorted the 12,998 hnRNP C PARCLIP-MeRIP peaks (with IP/Input enrichment ≥2) by the T-to-C mutation frequency. We then chose the top 4,500 peaks with the highest T-to-C mutation frequency for motif analysis using FIRE[38] with default RNA analysis parameters. The top two enriched motifs are the GRACH and the U-tract motif. We also used the top 1,024 and 2,048 peaks for motif analysis, yielding the same motif results as the top 4,500 peaks.

To identify transcriptome-wide hnRNP C m^{6}A-switches, we first searched for all coupling events within 50 nucleotides between U_5 and RRACH motif, with the U_5 motif located within hnRNP C binding sites. For PARCLIP-MeRIP samples, the fold change score E at the RRACH motif was calculated for each coupling event. Also, p-value for each coupling event was calculated as described[39]. Then, we generated the π-value, $\pi = E \cdot (-\log_{10} P)$, as one comprehensive parameter to pick meaningful genomic loci[40]. hnRNP C m^{6}A-switches identified from PARCLIP-MeRIP experiments should fulfill the following requirements: (i) read counts at both the control and IP sample ≥5; (ii) π-value ≥0.627, corresponding to FDR ≤5%.

For METTL KD samples, the fold change score at the U-tracts motif was calculated for each coupling event. hnRNP C m^{6}A-switches identified from *METTL3/L14* KD samples should fulfill the following requirements: (i) read counts at both the control and KD sample ≥5; (ii) π-value ≤0.627, corresponding to FDR ≤5%.

Distribution of hnRNP C m^{6}A-switches

Pie charts illustrating distribution within each segment were made using the following hierarchy: intron > ncRNA > 3′UTR > 5′UTR > CDS > intergenic. To plot the distribution of hnRNP C m^{6}A-switches in their respective localized segments (such as intron, exon, 3′UTR, CDS, 5′UTR), we first identified the distance between each m^{6}A-switch and the 5′ end of the respective segment. This distance was then divided by the length of that segment to determine a percentile where this m^{6}A-switch fell, and then this specific percentile bin

was incremented. Following this approach, we obtained the distribution pattern of all m^{6}A-switches within each segment.

RNA-seq

RNA-seq experiments were performed on two replicate RNA samples from *HNRNPC*, *METTL3*, *METTL14* KD as well as control HEK293T cells (48 hours after transfection). Total RNA samples were extracted according to RNeasy plus kit (Catalog # 74104, Qiagen). Libraries were prepared according to the TruSeq Stranded mRNA LT Sample Prep Kit (Catalog # RS-122-9005DOC). KD and control samples were sequenced together in one flowcell on four lanes, respectively. All samples were sequenced by illumina Hiseq 2000 with pair end 100-bp read length. The reads from the four lanes of each sample were combined for all analysis. The RNA-seq data was mapped using the splice-aware alignment algorithm TopHat version 1.1.4[41] based on the following parameters: tophat –num-threads 8 –mate-inner-dist 200 –solexa quals –min-isoform-fraction 0 –coverage-search-segment-mismatches 1. Gene expression level changes were analyzed using cuffdiff[42]. Differential splicing was determined using DEXSeq[30] based on Cufflinks-predicted, nonoverlapping exons. To compare with a different mRNA binding protein, the RNA-seq data from *HNRNPU* KD HEK293T cells (GEO34995 dataset[43]) was analyzed.

Gene Ontology, evolutionary conservation, graphic and statistical analysis

Gene Ontology (GO) enrichment analysis was applied on the co-regulated HCS-containing genes, against all HCS-containing genes as background, using GOrilla[44].

Phylogenetic conservation analysis was performed by comparing PhyloP scores at the U-tracts motif and RRACH motif for hnRNP C m^{6}A-switches to those of randomly selected sequences. The PhyloP scores were accessed from the precompiled phyloP scores[45] (ftp://hgdownload.soe.ucsc.edu/goldenPath/hg19/phyloP46way/) under both primates and vertebrates categories. P-values were evaluated using the Mann-Whitney-Wilcoxon test, ***: $p < 10^{-16}$. For the U-tract motifs, we collected all U-tracts (5x U's) across all chromosomes and randomly selected 10,000 sites among the 38,561,577 sites of our census. The random selection was done separately for primates and for vertebrates. For the RRACH motif, we also collected all RRACH sites across all chromosomes and randomly selected 10,000 sites among the 78,815,225 sites of our census. Here too, the random selection was done separately for primates and vertebrates.

Sequence logos were generated using the WebLogo package. R statistical package was used for all statistical analysis (unless stated otherwise).

Cell proliferation analysis

HEK293T cells were transfected with si-control, si-*HNRNPC*, si-*METTL3* and si-*METTL14* RNAs. After transfection, the numbers of cells were counted at 0, 24, 48 and 72 hrs as described in[46]. Three independent experiments were performed and growth curves were plotted to test the effects on cell proliferation.

RT-PCR quantitation

Total RNA samples were extracted from HEK293T cells and reverse transcribed using SuperScript® III First-Strand Synthesis System (Life Technologies, #18080-051). In order to validate the splicing changes identified from our RNA-seq data, we performed RT-PCR measurements using Thermo Scientific™ Taq™ DNA Polymerase under the following conditions: 95 °C for 3 mins, 30 cycles of [95 °C for 30 s, 55 °C for 30 s, 72 °C for 1 min] and then finally 72 °C for 10 min. For the target alternate exon, we designed and used primers annealing to both neighboring constitutive exons. The PCR products were separated on 1.2% agarose gel and ethidium bromide stained. In order to validate the gene expression level changes identified from our RNA-seq data, we performed qRT-PCR measurements using Power SYBR® Green PCR Master Mix (Life Technology, # 4367659) under the following conditions: 50 °C for 3 mins followed by 95 °C for 10 mins, 40 cycles of [95 °C for 15 s, 60 °C for 1 min] and then 40 °C for 1 min and 95 °C for 15 s and finally 60 °C for 30 s.

The primer sequences are listed as below (Gene name: forward primer; reverse primer): ANAPC1: TGCCAAAAGAAATAGCAGTTCAG; TGCCAAAAGAAATAGCAGTTCAG; ANLN: GCCAGGCGAGAGAATCTTCA; GGCTGCTGGTTACTTGCTTC; SRSF6: ACAAGGAACGAACAAATGAGGG; GCTTCCAGAGTAAGATCGCCTAT; E2F8: ACCCAAGCTCAGCCATTGTA; GAGTCATAGTTGGTGGCCCT; HIPK1: CCAGTCAGCTTTGTACCCATC; TTGAAACGCAGGTGGACATA; DNAJA3: CCCTTTCATTTGTACTGCCTCC; TGATCTCTTTCTGGCTGGCA; STAMBP: GTTCTCATCCCCAAGCAAAG; ATCCAGCCCAGTGTGATGA; ARHGAP5: GCGGATTCCATTTGACCTCC; GCTGCCCTGGTGAAATGAAT; ROBO1: TTTGGGCTTCTGCGTAGTTT; GGAGGGTACTGGAGACAGCA; SRPK1: CCCTGAGAAGAGAGCCACTG; ACCCTGAAAAGGGAAGAGGA; CENPK: AAGGCTAAAAATTCACAAAGCA; TCCATATCTTTCCACATTTCTTCA; BCLAF1: TCCTGAAAGGTCTGGGTCTG; TCCTGAAAGGTCTGGGTCTG; SUDS3: TGCCTGGGGTTCTGTATTTC; CAGTTCAAGCGAGGGAAGTC; DYRK1A: CTTCAGCATGCAAACCTTCA; GGCAGAAACCTGTTGGTCAC; SMEK1: TTGAAGGACTGCACCACTTG; CCTGTGTTTTCGTGGTTGTG; ATP6V1A: AAGCATTTCCCCTCTGTCAA; CTGCCAGGTCTTCTTCTTCC; KPNA6: CCCTGTGTTGATCGAAATCC; GATCTGCTCAGGGGTTCCTC; TBC1D23: GGTGAATCTCCTAATGGCTCA; CGATCCACAGGAGTTGATGT; GPBP1: CGTCATTGAATTTTGAGAAGCA; TTAGGACGCCCAATAGCAGA; MTF2: GTCTGCATTTGGTTCCTGGT; CTGCAGGAAAGGCAACCTTA; ATP6V0A1: TCCGTGTCTGGTTCATCAAA; TCTGAGTGCAAACTGGATGG; MAP4K3: TCTTCATACCACAGGAAATGC; AACAGGTTTGTGTGGGGGTA; SUMO2: TTCTTTCATTTCCCCCTTCC; TATTTTTCCCCATCCCGTCT; MAP3K3: CAGTTCCTCTCCCCACTCTG; GACAGAGAGGTGCCTGCTTC; CDS2: CGATTTTCCCAGGATGACAG; GAAAGGGCCCTATTGAGGAC; YTHDF2: ACTTGAGTCCACAGGCAAGG; AAGCAGCTTCACCCAAAGAA.

Extended Data

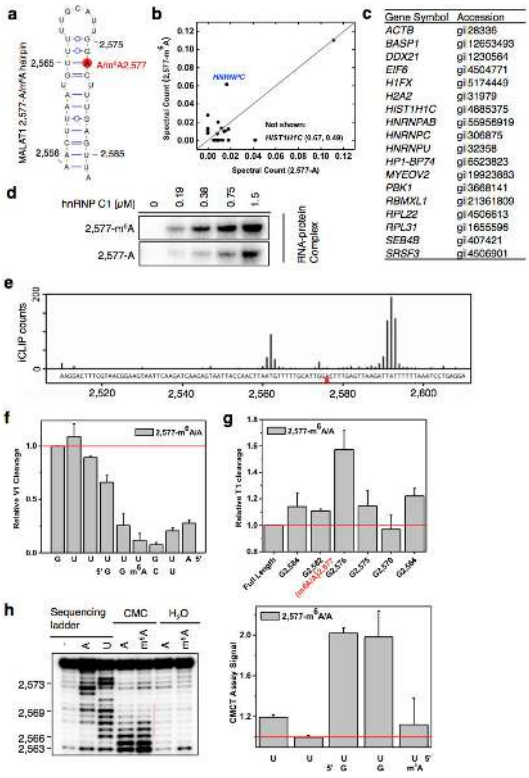

Extended Data Figure 1. m^{6}A increases the accessibility of U-tract to enhance hnRNP C binding

a, Secondary structure of the MALAT1 hairpin with m^{6}A methylation at 2,577 site shown in red[25]. Nucleotide position numbers correspond to their locations along the human MALAT1 transcript (NR_002819). **b,** RNA pull down showing hnRNP C preferably binds methylated RNA. **c,** The list of proteins with identified peptides by mass spectrometry in **b**. **d,** Recombinant hnRNP C1 binds stronger with MALAT1 2,577-m^{6}A hairpin compared to the unmethylated hairpin, as determined by *in vitro* UV crosslinking assay[23]. **e,** hnRNP C shows binding around A2,577 site along MALAT1 *in vivo*, as determined by previously published hnRNP C iCLIP data[20]. The underlying genomic sequence is shown at the bottom with a red square marking the m^{6}A2,577 site. The slight shift of the iCLIP signal to upstream of the U-tract binding site is likely due to the steric hindrance of the peptide fragment remaining on RNA which can cause reverse transcription to terminate more than one nucleotide upstream of the cross-link site[20]. **f,** Quantification of the RNase V1 cleavage signal for the U-tract region from RNA structural mapping assay in Fig. 1e. To correct for sample loading difference, each band signal was normalized to the band signal of the immediate 3' residue to the U-tract. n = 3, ± s.d., technical replicates. **g,** Quantitative of the RNase T1 cleavage signal from RNA structural mapping assay in Fig. 1e. Increased RNase T1 cleavage signal (single-stranded specific & cleavage after guanosines) was observed due to the surrounding m^{6}A residue. To correct for sample loading difference, the ratio for each band signal among all bands in each lane was calculated. The y-axis value Relative T1 cleavage = $(m^6A_{native}/m^6A_{denature})/(A_{native}/A_{denature})$. n = 2, technical replicates. **h,** Quantitative CMCT mapping showing increased signals for the U-tract bases around the U base-pairing with

m^{6}A. Quantitation of band signals within the U-tract region is shown on the right. n = 4, ± s.d., technical replicates.

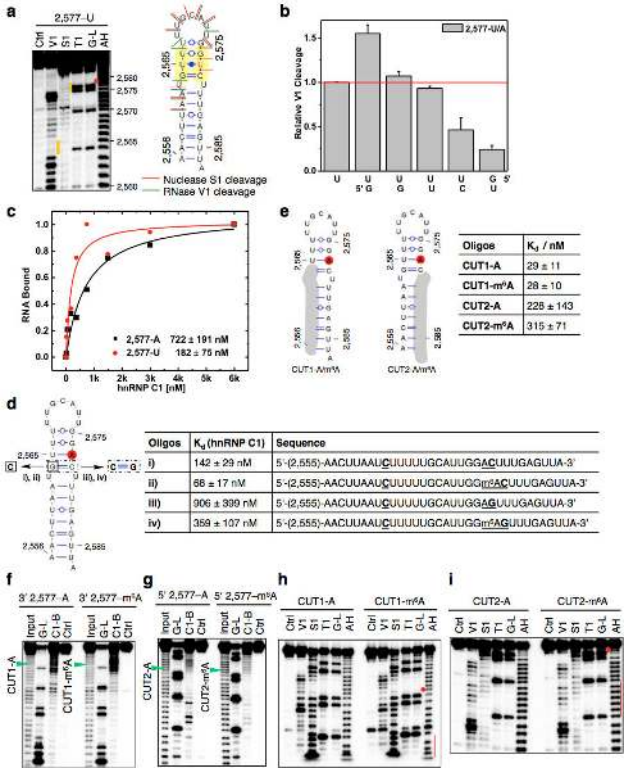

Extended Data Figure 2. Increased accessibility of U-tracts enhances hnRNP C binding

a, Structure probing of the 2,577A-to-U mutated MALAT1 hairpin (2,577-U), same annotation as in Fig. 1d. **b,** Quantification of the RNase V1 cleavage signal for the U-tract region from RNA structural mapping assays as in **a**. To correct for sample loading difference, each band signal was normalized to the band signal of the 3' most U of the U-tract. n = 2, technical replicates. **c,** Filter-binding curves displaying the binding affinities between recombinant hnRNP C1 and 2,577-U/A oligos. n = 3, ± s.d., technical replicates. **d,** Filter-binding results showing the binding affinities between recombinant hnRNP C1 and four mutated MALAT1 oligos. (i) Mutate G-C to C-C, A2,577: predicted to weaken the hairpin stem and increase hnRNP C binding. Results: binding improved from 722 nM K_d to 142 nM (5-fold); (ii) Mutate G-C to C-C, m^{6}A2,577: in this context of weaker stem, m^{6}A is predicted to confer a smaller effect compared to wild-type hairpin. Result: improved binding only 2-fold instead of 8-fold; (iii) Restore C-C to C-G, A2,577: predicted to restore the hairpin stem and decrease hnRNP C binding compared to C-C mutant. Result: binding decreased by 6.4-fold; (iv) Restore C-C to C-G, m^{6}A2,577: in this context of restored stem, m^{6}A is again predicted to confer increased binding compared to A2,577 hairpin. Result: improved binding by 2.5-fold. n = 3 each, ± s.d., technical replicates. **e,** RNA alkaline hydrolysis terminal truncation assay showing recombinant hnRNP C1 binding to terminal truncated MALAT1 hairpin oligos (2,577 site m^{6}A methylated or unmethylated). In this assay, 3′ radiolabeled MALAT1 2,577 hairpin oligos were terminal truncated by alkaline hydrolysis into RNA fragments which were then incubated with hnRNP C1 protein followed

by filter binding wash steps. The remaining RNA on the filter paper was isolated and analyzed by denaturing gel electrophoresis, as indicated in the lane "C1-bound or C1-B". "Input" refers to alkaline hydrolysis truncated RNA oligos used for incubation with hnRNP C1; "G-L or G-ladder" was generated from RNase T1 digestion; "Ctrl" refers to the intact MALAT1 hairpin without alkaline hydrolysis truncation. One pair of methylated/unmethylated truncated oligos (CUT1, marked by green arrows) was selected for subsequent biochemical analysis, due to their strong interaction with hnRNP C1. **f,** RNA terminal truncation assay as in **e** except 5′ ^{32}P-labeled oligos were used. One pair of methylated/unmethylated truncated oligos (CUT2, marked by green arrows) was selected for subsequent biochemical analysis. **g**, Structure probing of the CUT1 oligos using RNase V1 and nuclease S1 digestion, same annotation as in Fig. 1e. The red dot marks the m^{6}A site and the red line marks the U-tract region. **h,** Structure probing of the CUT2 oligos using RNase V1 and nuclease S1 digestion, same annotation as in **g**. **i,** Truncated oligos with exposed U-tracts increased hnRNP C binding regardless of m^{6}A. n = 3, ± s.d., technical replicates.

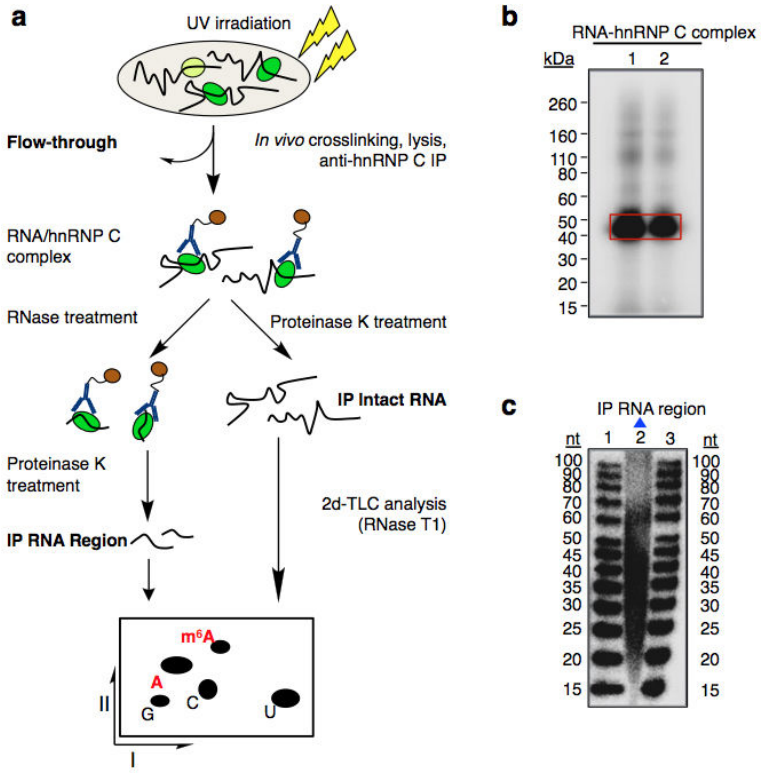

Extended Data Figure 3. m^{6}A is enriched in the vicinity of hnRNP C binding sites

a, Schematic diagram of the CLIP-2dTLC protocol. IP, immunoprecipitation; nt, nucleotide. The RNase T1 used in our 2dTLC assay cleaves single-stranded RNA after guanosines, so the m^{6}A/A ratio determined here represents the m^{6}A fraction of all adenosines following guanosines. **b**, Analysis of crosslinked RNA-hnRNP C complexes (CLIP RNP) using denaturing gel electrophoresis (lanes 1 and 2). Positions of the protein size standards are shown on the left. hnRNP C IP RNA region (RNA samples within RNA-hnRNP C crosslinked complexes) were extracted from the gel slices marked by the red rectangle. **c,**

Denaturing gel analyzing the size distribution for the hnRNP C PAR-CLIP RNA samples (lane 2). The RNA size standards were loaded in lanes 1 and 3.

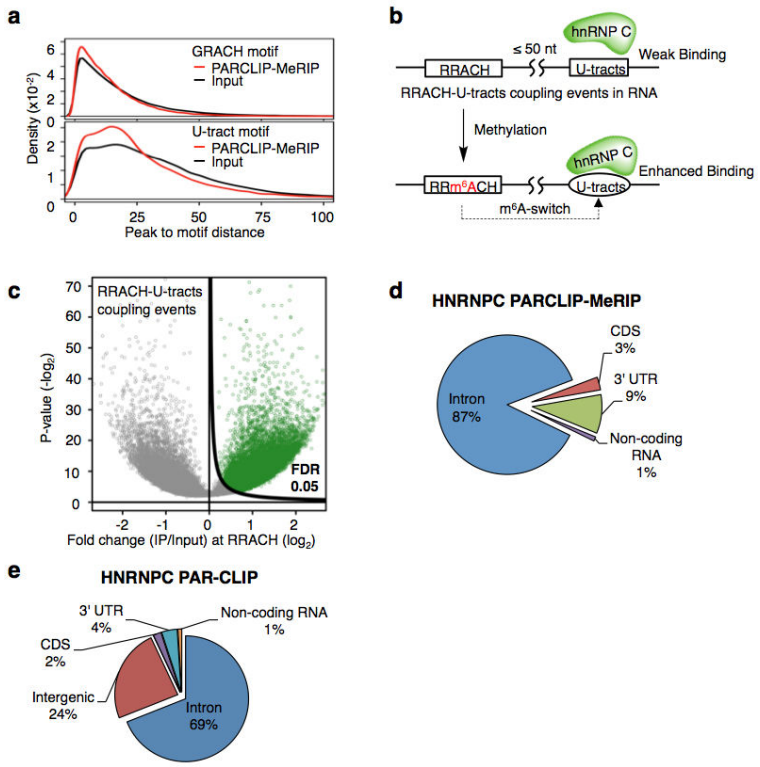

Extended Data Figure 4. PARCLIP-MeRIP identifies transcriptome-wide m^{6}A-switches in the vicinity of hnRNP C binding sites

a, Density plots illustrating the distribution of distance between the PARCLIP-MeRIP/Input peaks and the nearest GRACH motif (top) or the nearest U-tracts in (bottom). **b**, Definition and identification of hnRNP C m^{6}A-switches based on the PARCLIP-MeRIP analysis. Approximately 89% of PARCLIP-MeRIP peaks harboring both the U-tract and RRACH motif have “RRACH-U-tract” inter-motif distance within 50 nucleotides, significantly higher than the 64% of such coupling within the genomes. hnRNP C m^{6}A-switches are identified as m^{6}A methylated RRACH-U-tracts coupling events. **c,** Volcano plot depicting all coupling events (unfilled circles) as defined in **b**, according to their p-values[37] (P, y-axis) and fold change values at RRACH sites (E, x-axis). To identify hnRNP C m^{6}A-switches, we generated the π-value, π=E·(-log$_{10}$P), as one comprehensive parameter to pick meaningful genomic loci[38]. hnRNP C m^{6}A-switches identified from PARCLIP-MeRIP experiments should fulfill the following requirements: (i) read counts at both the control and IP sample ≥ 5; (ii) π-value ≥0.627, corresponding to False Discovery Rate (FDR) ≤5%. **d,** Pie chart depicting the region distribution of hnRNP C m^{6}A-switches identified by PARCLIP-MeRIP. **e,** Pie chart depicting hnRNP C PAR-CLIP peaks. These are enriched in introns, consistent with previous reports that hnRNP C binds mainly nascent transcripts[19,23,25].

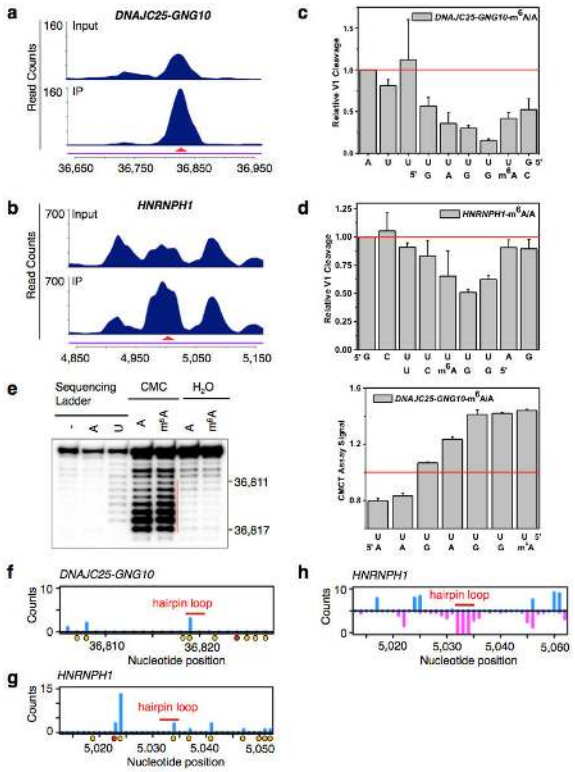

Extended Data Figure 5. Validation of two identified m^{6}A-switches

a-b, PARCLIP-MeRIP data detected positive IP/Input enrichment at the RRACH sites (red arrowheads) on the *DNAJC25-GNG10* gene (**a**) and *HNRNPH1* gene (**b**) in HEK293T cells. **c-d**, Quantification of RNase V1 cleavage signals around the U-tract region of m^{6}A-switches on the *DNAJC25-GNG10* (**c**) and *HNRNPH1* (**d**) transcript, related to Fig. 2g-h. n = 3, ± s.d., technical replicates each. **e,** Quantitative CMCT mapping of *DNAJC25-GNG10* m^{6}A-switch shows increased band signals around the uridine base that pairs with m^{6}A. The red vertical line marks the U-tract region. Quantitation of bands signal for the U-tract region is shown on the right. n = 3, ± s.d., technical replicates. *HNRNPH1* m^{6}A-switch hairpin is not suitable for CMCT probing, because its reverse transcription binding primer region is too short. **f-g,** *In vivo* DMS mapping of the *DNAJC25-GNG10* hairpin (**f**) and *HNRNPH1* (**g**); data are from[7]. A and C residues are marked with orange dots and the m^{6}A residue is marked with a red dot. The hairpin loops are indicated by red bars. **h,** Transcriptome-wide S1/V1 mapping around the *HNRNPH1* m^{6}A-switch site. Blue bars represent V1 signal; magenta bars represent S1 signal. The hairpin loop is indicated by a red bar; data are from[4]. Not enough reads could be collected to make a plot for the *DNAJC25-GNG10* m^{6}A-switch region.

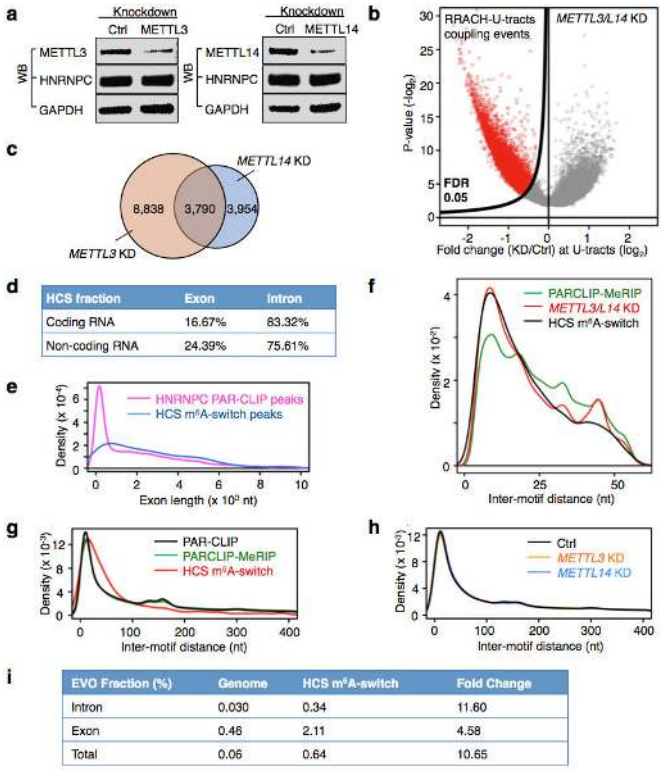

Extended Data Figure 6. Molecular features of HCS m^{6}A-switches

a, Western blot showing stable hnRNP C protein abundance upon *METTL3/L14* KD. **b,** Volcano plot of the *METTL3/L14* KD data depicting RRACH-U-tracts coupling events (unfilled red circles) as defined in Extended Data Fig. 4b, according to their p-values[39] (P, y-axis) and fold change values at the U-tracts (E, x-axis). **c,** Overlap of RRACH-U-tract coupling events with decreased hnRNP C binding by *METTL3* and *METTL14* KD. **d,** The intron fraction of HCS m^{6}A-switches in coding RNA and non-coding RNA. **e,** Density plot displaying the distribution of exonic m^{6}A-switches/HNRNPC PAR-CLIP peaks according to exon length. **f,** Inter-motif (RRACH-U-tract) distance distributions suggest that m^{6}A-switches have a preference for shorter distances between the RRACH and U-tract (> 5xU) motifs. The distribution curves are from PARCLIP-MeRIP data (green), *METTL3/L14* KD (red) and HCS m^{6}A-switches (black). **g,** Analysis of the inter-motif (U-tract-U-tract) distance patterns, previously identified by iCLIP[20], in PARCLIP-MeRIP, *METTL3/L14* KD and HCS m^{6}A-switch data. The peaks at ~165 and ~300 nucleotides are clearly present. For the 2,798 high confident switches, we analyzed those in which the other U-tract motif is also in a PAR-CLIP-identified sequence; the long-range peaks seem to have shifted to longer distances (~220 and ~370 nucleotides). **h,** *METTL3/L14* KD does not affect the inter-motif (U-tract-U-tract) distance distributions for U-tracts (≥5x U) in HEK293T cells. **i,** EVOfold analysis for the 2,798 HCS m^{6}A-switches. The chances for HCS m^{6}A-switches to have EVOfold records are significantly higher than random genomic sequences. We first calculated the number of HCS sites in the EVO database if occurring in random to be ~1.7 HCS sites. We found 18 HCS sites are present in EVO database, resulting in ~11x enrichment. This result is further divided into intronic and exonic regions.

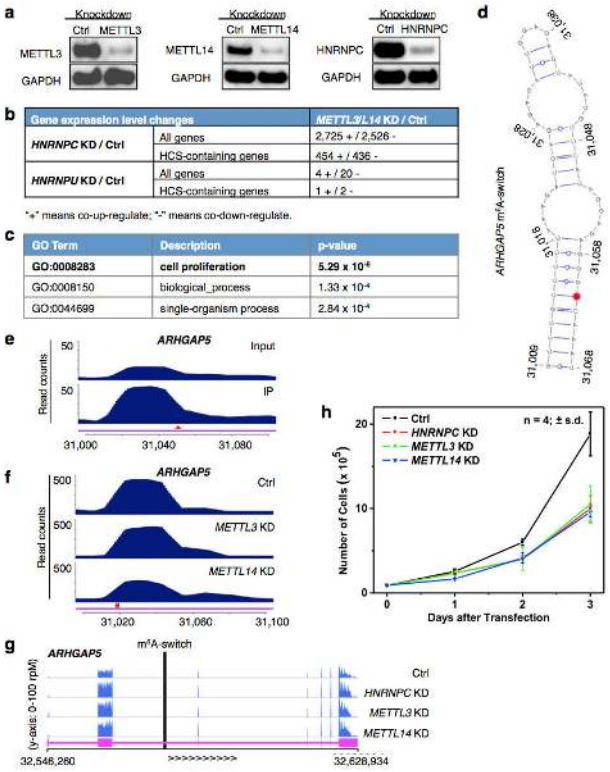

Extended Data Figure 7. m^{6}A-switches regulate the abundance of target mRNAs

a, *HNRNPC*, *METTL3/L14* KD confirmed by Western blots. **b,** *HNRNPC* KD and *METTL3/L14* KD co-regulated the expression of a large number of genes. Gene expression changes between Ctrl and *HNRNPC*, *HNRNPU*, *METTL3/L14* KD HEK293T cells were analyzed by Cuffdiff2[39,40], and the absolute numbers of differential expressed genes are shown. HCS-containing genes refer to the 1815 genes containing high confident m^{6}A-switches. The RNA-seq data from *HNRNPU* KD HEK293T cells (GEO34995 dataset[41]) was analyzed for comparison with a different mRNA binding protein. HnRNPU did not show preferential interaction with the 2,577-m^{6}A modified MALAT1 hairpin (Fig. 1b, 1c). **c,** Gene ontology analysis of the m^{6}A-switch-containing genes whose expression level were co-differentially-regulated by *HNRNPC* and *METTL3/L14* KD, against all m^{6}A-switch-containing genes as background. **d,** An example of m^{6}A-switch among co-regulated transcript is the *ARHGAP5* transcript (NM_001030055). Its proposed secondary structure with m^{6}A methylation site in red is shown with the opposing the U-tract in a stem. **e-f,** PARCLIP-MeRIP detected positive IP/Input enrichment at the RRACH site (red arrowhead) of the *ARHGAP5* m^{6}A-switch (**e**), while *METTL3/L14* KD decreased hnRNP C binding at the U-tract (red square) of this m^{6}A-switch (**f**). **g,** The expression level of *ARHGAP5* gene was co-upregulated by *HNRNPC*, *METTL3/L14* KD, as shown by the RNA-seq data from HEK293T cells. The vertical black line represents the m^{6}A-switch site. **h,** *HNRNPC*, *METTL3/L14* KD decreased the proliferation rates of HEK293T cells to a similar extent. n = 4, ± s.d., biological replicates.

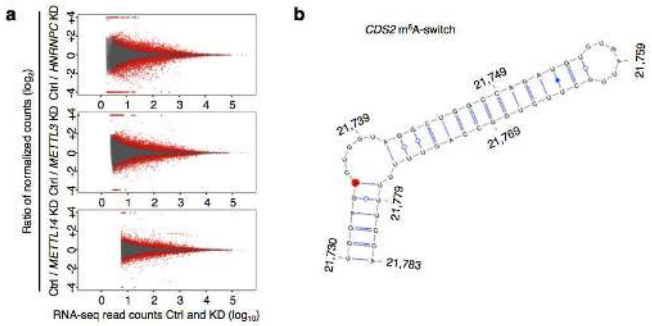

g

Exon/Intron junction rate (reads per million)		p-value, Chi-Square test
Control	169	--
HNRNPC KD	161	1.1×10^{-13}
METTL3 KD	154	2.8×10^{-43}
METTL14 KD	156	1.6×10^{-39}

"--" meaningless in the Chi-Square test with itself.

Extended Data Figure 8. m^{6}A-switches regulate alternative splicing of target mRNAs

a, Fold changes (KD/Ctrl, $\log_2$) in normalized exon expression against RNA-seq reads detect the exons in *HNRNPC* KD, *METTL3* KD, *METTL14* KD and control samples. Statistically Significant Differentially Expressed Exons (SSDEE) called by DEXSeq are indicated in red. **b**, Proposed secondary structure of the *CDS2* hairpin with the m^{6}A methylation site shown in red, opposing the U-tract region. Nucleotide position numbers correspond to their locations along the human *CDS2* transcript (NM_003818). **c,** Proposed secondary structure of the *YTHDF2* hairpin with the m^{6}A methylation site shown in red, opposing the U-tract region. Nucleotide position numbers correspond to their locations along the human *YTHDF2* transcript (NM_001173128). **de,** PARCLIP-MeRIP detected a positive enrichment at the RRACH site (red arrowhead) (**d**), while *METTL3/L14* KD decreased hnRNP C binding at the U-tract (red square) of this *YTHDF2* m^{6}A-switch (**e**). **f,** The inclusion level of one *YTHDF2* exon is co-down-regulated by *HNRNPC* KD, *METTL3* KD and *METTL14* KD, as validated by RT-PCR. n = 3, ± s.d., biological replicates. **g,** We analyzed our polyA$^+$ RNA-seq data to look for reads that span intron/exon junctions on CDS m^{6}A-switch containing genes. We find that the control sample has significantly higher reads spanning intron/exon junctions than *HNRNPC*, *METTL3/L14* KD samples. This result indicates that m^{6}A depletion at the CDS m^{6}A-switches promotes intron exclusion.

a

Experiment	Sample/replicates	Mapped reads	T-to-C mutation rate
PARCLIP-MeRIP	Input-rep1	28,755,227	0.67
	Input-rep2	34,022,750	0.67
	IP-rep1	22,515,468	0.83
	IP-rep2	48,570,954	0.76
PAR-CLIP	Ctrl-rep1	22,728,884	0.69
	Ctrl-rep2	24,827,034	0.75
	METTL3 KD-rep1	19,697,397	0.67
	METTL3 KD-rep2	31,864,420	0.75
	METTL14 KD-rep1	20,835,499	0.67
	METTL14 KD-rep2	20,102,049	0.71

b

Experiment	Sample/replicates	Total reads	Mapped reads	Mapped rate
RNA-seq	Ctrl-rep1	78,453,301	68,058,093	86.70%
	Ctrl-rep2	78,823,710	70,907,544	90.00%
	*HNRNPC*_KD-rep1	81,933,883	72,840,271	88.90%
	*HNRNPC*_KD-rep2	78,133,137	68,053,888	87.10%
	*METTL3*_KD-rep1	58,140,943	48,123,493	82.80%
	*METTL3*_KD-rep2	58,923,206	53,011,571	90.00%
	*METTL14*_KD-rep1	77,932,017	68,703,305	88.20%
	*METTL14*_KD-rep2	75,442,883	65,812,269	87.20%

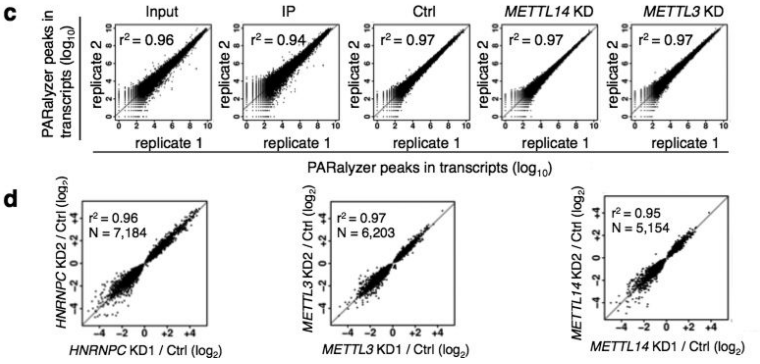

Extended Data Figure 9. Summary of the sequencing samples

a, For PARCLIP-MeRIP and PAR-CLIP experiments from HEK293T cells, the number of mapped reads and "T-to-C" mutation rates are given for each replicate. **b**, For RNA-seq experiments from HEK293T cells, the number of total reads, the number of mapped reads as well as the mapping rates is given for each replicate. **c,** Scatter plots comparing transcripts for all PAR-CLIP replicate experiments. The square of Spearman's rank correlation value (r^2) for each pair is shown in the upper left corner of the respective panel. **d,** The detected expression level changes show a strong correlation between gene KD replicates. Scatter plots comparing the fold changes (log_2) in normalized gene expression from replicates of *HNRNPC*, *METTL3* and *METTL14* KD. The square of Spearman's rank correlation value (r^2) for each pair is shown in the upper left corner of respective panels.

Acknowledgements

This work is supported by National Institutes of Health EUREKA GM088599 (C.H. and T.P.). We thank all members of the Pan and He laboratories for comments and discussions. We also thank Drs. Y.C. Leung, G. Perdrizet, Y. Pigli, J. Yue, J. Liu, Y. Yue, K. Chen and M. Yu for technical assistance. M.P. was a Natural Sciences and Engineering Research Council of Canada postdoctoral fellow.

References

1. Antson AA. Single-stranded-RNA binding proteins. Curr Opin Struct Biol. 2000; 10:87–94. [PubMed: 10679466]
2. Dreyfuss G, Kim VN, Kataoka N. Messenger-RNA-binding proteins and the messages they carry. Nat Rev Mol Cell Biol. 2002; 3:195–205. [PubMed: 11994740]
3. Ray D, et al. A compendium of RNA-binding motifs for decoding gene regulation. Nature. 2013; 499:172–177. [PubMed: 23846655]

4. Wan Y, et al. Landscape and variation of RNA secondary structure across the human transcriptome. Nature. 2014; 505:706–709. [PubMed: 24476892]
5. Ding Y, et al. *In vivo* genome-wide profiling of RNA secondary structure reveals novel regulatory features. Nature. 2013; 505:696–700. [PubMed: 24270811]
6. Kertesz M, et al. Genome-wide measurement of RNA secondary structure in yeast. Nature. 2010; 467:103–107. [PubMed: 20811459]
7. Rouskin S, Zubradt M, Washietl S, Kellis M, Weissman JS. Genome-wide probing of RNA structure reveals active unfolding of mRNA structures *in vivo*. Nature. 2013; 505:701–705. [PubMed: 24336214]
8. Bokar, JA. The biosynthesis and functional roles of methylated nucleosides in eukaryotic mRNA. Fine-tuning of RNA functions by modification and editing. Grosjean, H., editor. Springer-Verlag; Berlin, Heidelberg, New York: 2005. p. 141-178.
9. Jia G, et al. N^6-methyladenosine in nuclear RNA is a major substrate of the obesity-associated FTO. Nat Chem Biol. 2011; 7:885–887. [PubMed: 22002720]
10. Zheng G, et al. ALKBH5 is a mammalian RNA demethylase that impacts RNA metabolism and mouse fertility. Mol Cell. 2013; 49:18–29. [PubMed: 23177736]
11. Liu J, et al. A METTL3-METTL14 complex mediates mammalian nuclear RNA N^{6-} adenosine methylation. Nat Chem Biol. 2014; 10:93–95. [PubMed: 24316715]
12. Wang Y, et al. N^6-methyladenosine modification destabilizes developmental regulators in embryonic stem cells. Nat Cell Biol. 2014; 16:191–198. [PubMed: 24394384]
13. Dominissini D, et al. Topology of the human and mouse m^6A RNA methylomes revealed by m^6A-seq. Nature. 2012; 485:201–206. [PubMed: 22575960]
14. Meyer KD, et al. Comprehensive analysis of mRNA methylation reveals enrichment in 3′ UTRs and near stop codons. Cell. 2012; 149:1635–1646. [PubMed: 22608085]
15. Wang X, et al. N^6-methyladenosine-dependent regulation of messenger RNA stability. Nature. 2014; 505:117–120. [PubMed: 24284625]
16. Fustin JM, et al. RNA-methylation-dependent RNA processing controls the speed of the circadian clock. Cell. 2014; 155:793–806. [PubMed: 24209618]
17. Schwartz S, et al. High-resolution mapping reveals a conserved, widespread, dynamic mRNA methylation program in yeast meiosis. Cell. 2014; 155:1409–21. [PubMed: 24269006]
18. Batista P, et al. m^6A RNA modification controls cell fate transition in mammalian embryonic stem cells. Cell Stem Cell. 2014; 15:707–719. [PubMed: 25456834]
19. Zhao X, et al. FTO-dependent demethylation of N^6-methyladenosine regulates mRNA splicing and is required for adipogenesis. Cell Res. 2014; 24:1403–1419. [PubMed: 25412662]
20. Konig J, et al. iCLIP reveals the function of hnRNP particles in splicing at individual nucleotide resolution. Nat Struct Mol Biol. 2010; 17:909–915. [PubMed: 20601959]
21. McCloskey A, Taniguchi I, Shinmyozu K, Ohno M. hnRNP C tetramer measures RNA length to classify RNA polymerase II transcripts for export. Science. 2012; 335:1643–1646. [PubMed: 22461616]
22. Rajagopalan LE, Westmark CJ, Jarzembowski JA, Malter JS. hnRNP C increases amyloid precursor protein (APP) production by stabilizing APP mRNA. Nucleic Acids Res. 1998; 26:3418–3423. [PubMed: 9649628]
23. Zarnack K, et al. Direct competition between hnRNP C and U2AF65 protects the transcriptome from the exonization of Alu elements. Cell. 2012; 152:453–466. [PubMed: 23374342]
24. Cieniková Z, et al. Structural and Mechanistic Insights into Poly(uridine) Tract Recognition by the hnRNP C RNA Recognition Motif. J. Am. Chem. Soc. 2014; 136:14536–14544. [PubMed: 25216038]
25. Liu N, et al. Probing N^6-methyladenosine RNA modification status at single nucleotide resolution in mRNA and long noncoding RNA. RNA. 2013; 19:1848–1856. [PubMed: 24141618]
26. Krecic AM, Swanson MS. hnRNP complexes: composition, structure, and function. Curr Opin Cell Biol. 1999; 11:363–371. [PubMed: 10395553]

27. Gorlach M, Burd CG, Dreyfuss G. The determinants of RNA-binding specificity of the heterogeneous nuclear ribonucleoprotein C proteins. J Biol Chem. 1994; 269:23074–23078. [PubMed: 8083209]
28. Kierzek E, Kierzek R. The thermodynamic stability of RNA duplexes and hairpins containing N^6-alkyladenosines and 2-methylthio-N^6-alkyladenosines. Nucleic Acids Res. 2003; 31:4472–4480. [PubMed: 12888507]
29. Hafner M, et al. Transcriptome-wide identification of RNA-binding protein and microRNA target sites by PAR-CLIP. Cell. 2010; 141:129–141. [PubMed: 20371350]
30. Anders S, Reyes A, Huber W. Detecting differential usage of exons from RNA-seq data. Genome Res. 2012; 22:2008–2017. [PubMed: 22722343]
31. Gorlach M, Burd CG, Dreyfuss G. The determinants of RNA-binding specificity of the heterogeneous nuclear ribonucleoprotein C proteins. J Biol Chem. 1994; 269:23074–23078. [PubMed: 8083209]
32. Ehresmann C, et al. Probing the structure of RNAs in solution. Nucleic Acids Res. 1987; 15:9109–9128. [PubMed: 2446263]
33. Peterson ET, Pan T, Coleman J, Uhlenbeck OC. *In vitro* selection of small RNAs that bind to Escherichia coli phenylalanyl-tRNA synthetase. J Mol Biol. 1994; 242:186–192. [PubMed: 8089840]
34. Corcoran DL, et al. PARalyzer: definition of RNA binding sites from PAR-CLIP short-read sequence data. Genome Biol. 2011; 12:R79. [PubMed: 21851591]
35. Dominissini D, Moshitch-Moshkovitz S, Salmon-Divon M, Amariglio N, Rechavi G. Transcriptome-wide mapping of N^6-methyladenosine by m^6A-seq based on immunocapturing and massively parallel sequencing. Nat Protoc. 2013; 8:176–189. [PubMed: 23288318]
36. Lohse M, et al. RobiNA: a user-friendly, integrated software solution for RNA-Seq-based transcriptomics. Nucleic Acids Res. 2012; 40:W622–627. [PubMed: 22684630]
37. Langmead B, Trapnell C, Pop M, Salzberg SL. Ultrafast and memory-efficient alignment of short DNA sequences to the human genome. Genome Biol. 2009; 10:R25. [PubMed: 19261174]
38. Elemento O, Slonim N, Tavazoie S. A universal framework for regulatory element discovery across all genomes and data types. Mol Cell. 2007; 28:337–350. [PubMed: 17964271]
39. Ouyang Z, Snyder MP, Chang HY. SeqFold: genome-scale reconstruction of RNA secondary structure integrating high-throughput sequencing data. Genome Res. 2013; 23:377–387. [PubMed: 23064747]
40. Xiao Y, et al. A novel significance score for gene selection and ranking. Bioinformatics. 2012; 30:801–807. [PubMed: 22321699]
41. Trapnell C, Pachter L, Salzberg SL. TopHat: discovering splice junctions with RNA-Seq. Bioinformatics. 2009; 25:1105–1111. [PubMed: 19289445]
42. Trapnell C, et al. Differential gene and transcript expression analysis of RNA-seq experiments with TopHat and Cufflinks. Nat Protoc. 2012; 7:562–578. [PubMed: 22383036]
43. Huelga SC, et al. Integrative genome-wide analysis reveals cooperative regulation of alternative splicing by hnRNP proteins. Cell Rep. 1:167–178. [PubMed: 22574288]
44. Eden E, Navon R, Steinfeld I, Lipson D, Yakhini Z. GOrilla: a tool for discovery and visualization of enriched GO terms in ranked gene lists. BMC Bioinformatics. 2009; 10:48. [PubMed: 19192299]
45. Pollard KS, Hubisz MJ, Rosenbloom KR, Siepel A. Detection of nonneutral substitution rates on mammalian phylogenies. Genome Res. 2010; 20:110–121. [PubMed: 19858363]
46. Yang F, Yi F, Han X, Du Q, Liang Z. MALAT-1 interacts with hnRNP C in cell cycle regulation. FEBS Lett. 2013; 587:3175–3181. [PubMed: 23973260]

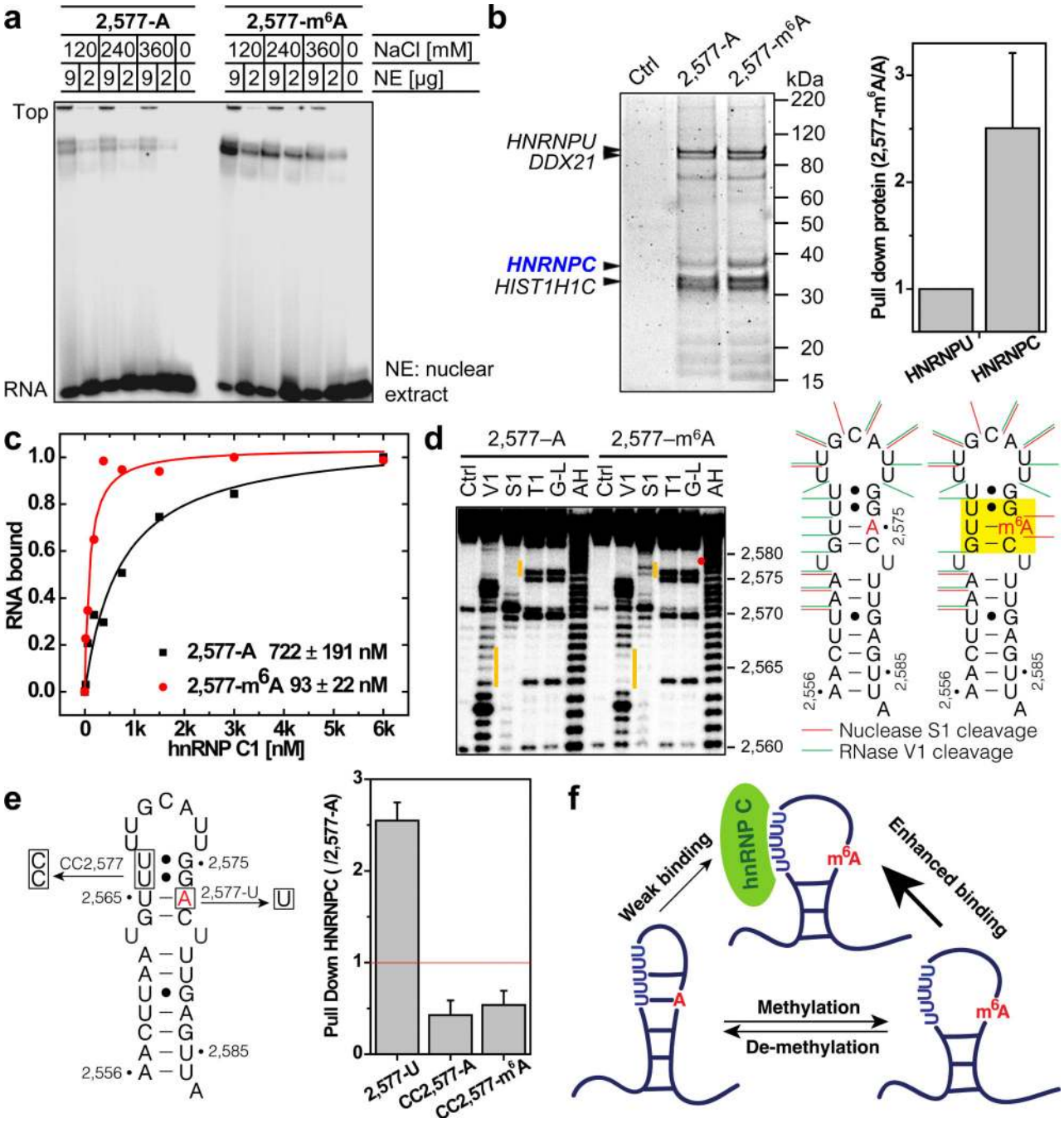

Figure 1. m^{6}A alters RNA structure to enhance hnRNP C binding

a, m^{6}A increases binding with nuclear proteins. **b,** RNA pull down showing hnRNP C preferably binds methylated RNA. n = 4, ± s.d., biological replicates. **c,** Filter binding showing m^{6}A increases hnRNP C1 binding with respective apparent dissociation constant (K_d) indicated at lower right; n = 3, ± s.d., technical replicates. **d,** RNA structural probing showing m^{6}A disrupts local RNA structure highlighted in yellow. Ctrl, no nuclease added; V1, RNase V1 digestion; S1, nuclease S1 digestion; T1, RNase T1 digestion; G-L, G-ladder; AH, alkaline hydrolysis. The orange bars mark the structurally altered RNA regions in the

presence of m^6A (red dot). **e,** RNA pull down with mutated oligos. n = 3, ± s.d., technical replicates. **f,** Illustration of the m^6A-switch model.

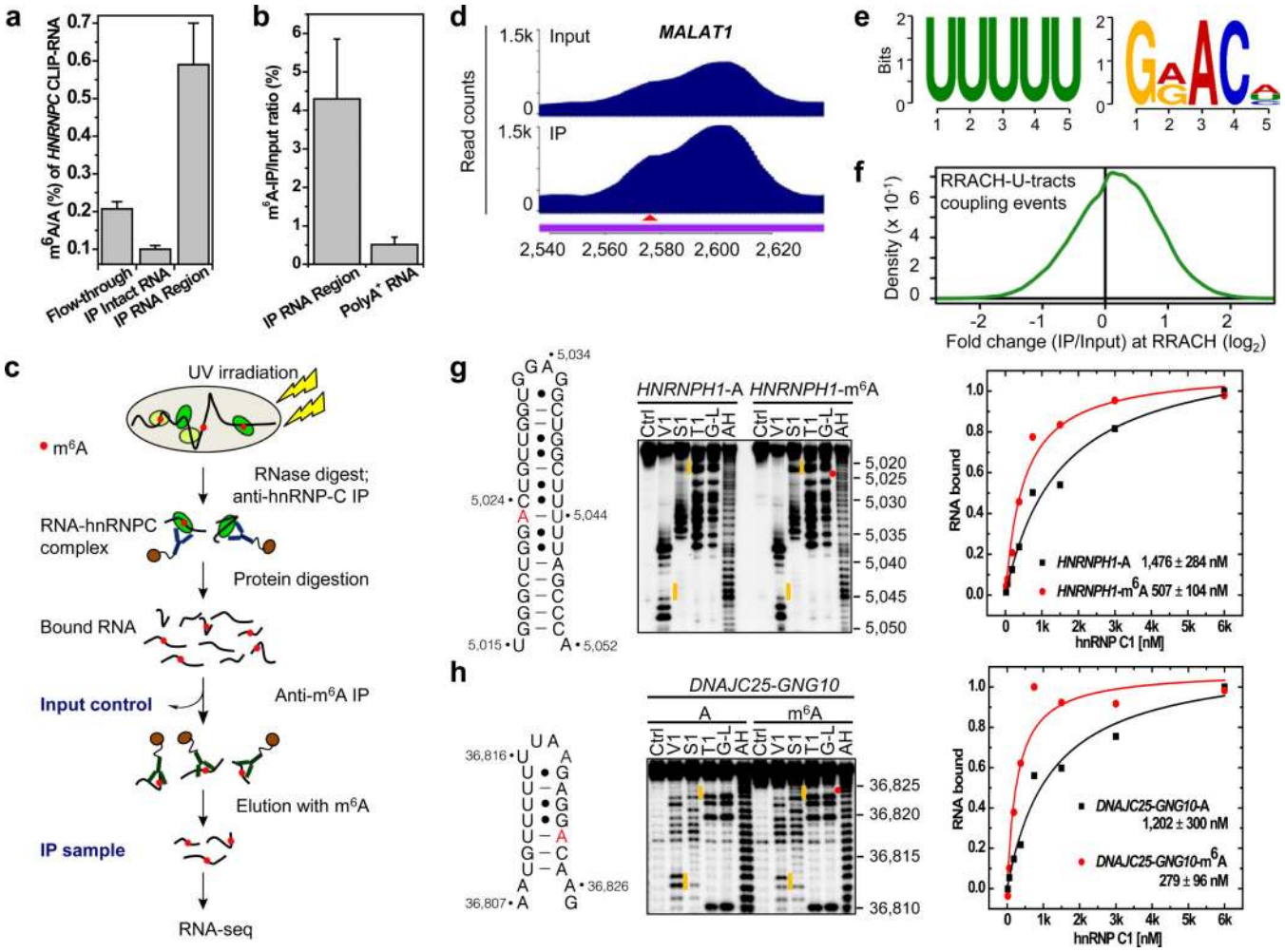

Figure 2. PARCLIP-MeRIP identifies m^{6}A-switches transcriptome-wide

a, CLIP-2dTLC showing the m^{6}A enrichment in hnRNP C bound RNA regions. n = 3, ± s.d., biological replicates. **b,** hnRNP C bound RNA regions had higher anti-m^{6}A pull down yield than polyA$^+$ RNA. n = 3, ± s.d., biological replicates. **c,** Illustration of the PARCLIP-MeRIP protocol. IP, immunoprecipitation. **d,** PARCLIP-MeRIP identified m^{6}A residue around the MALAT1 2,577 site. **e,** Binding motifs identified by FIRE with PARCLIP-MeRIP peaks. **f,** Density plot showing the positive enrichment at RRACH sites. **g-h,** Validation of two m^{6}A-switches by S1/V1 structural probing and filter binding. n = 4, ± s.d., technical replicates. Same annotation as in Fig. 1c, d.

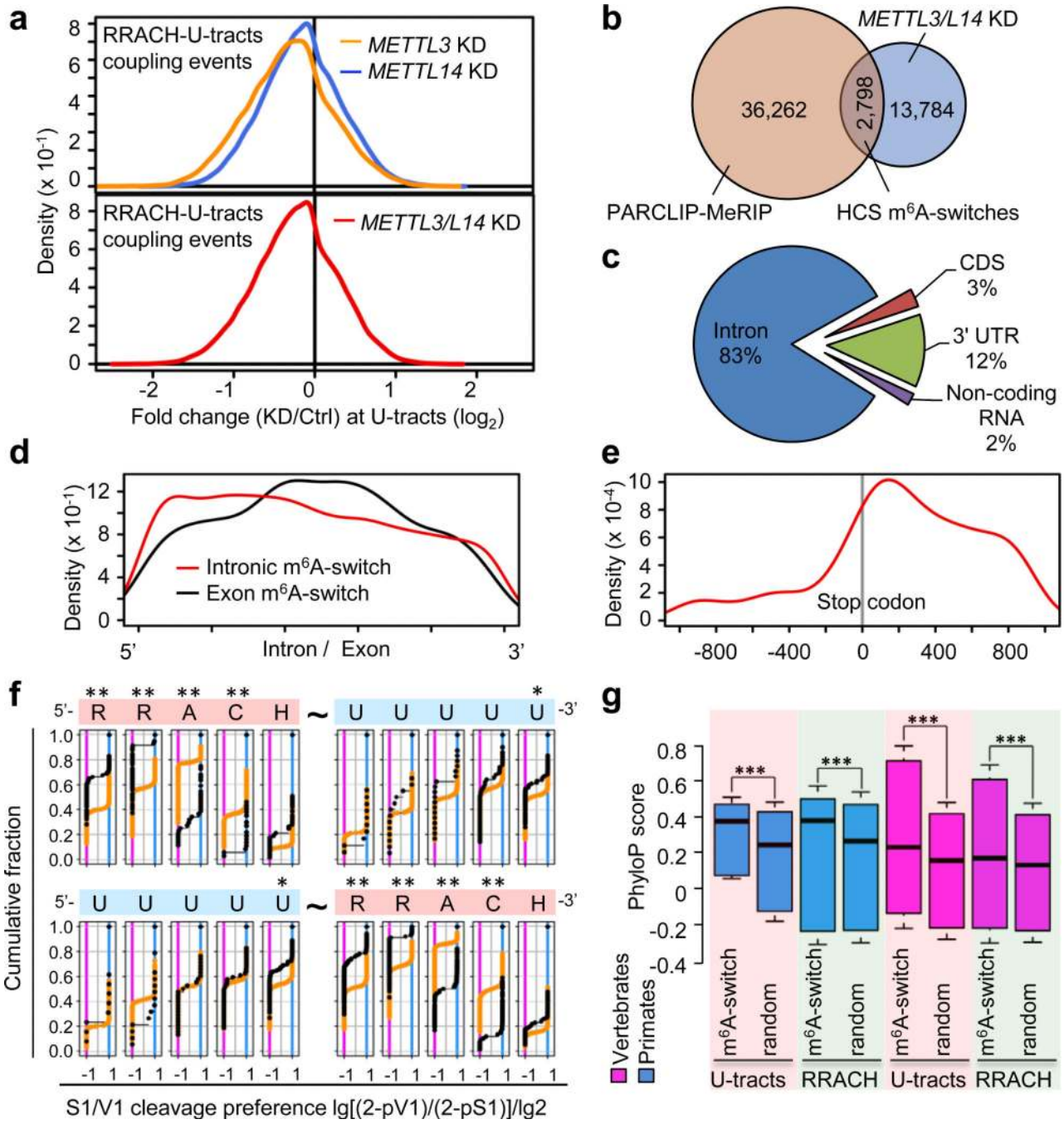

Figure 3. Global m^{6}A reduction decreases hnRNP C binding at m^{6}A-switches

a, Density plot showing negative enrichment at the U-tracts. **b,** Identification of HCS m^{6}A-switches. **c,** Region distribution of HCS m^{6}A-switches. **d,** Density plot showing m^{6}A-switches distribution relative to exon/intron boundaries. **e,** m^{6}A-switches in coding RNA were enriched in the 3'UTR and near the stop codon. **f,** Cumulative distribution of HCS m^{6}A-switches (black) and control (orange) regarding the S1/V1 cleavage preference (data from[4]) at U-tracts and RRACH motif. U-tract can be 3' (upper) or 5' (lower) of the RRACH motif. *: $p < 0.05$, **: $p < 10^{-4}$, Kolmogorov-Smirnov test. **g,** Phylogenetic conservation of

HCS m^6A-switches among primates and vertebrates. ***: $p < 10^{-16}$, Mann-Whitney-Wilcoxon test.

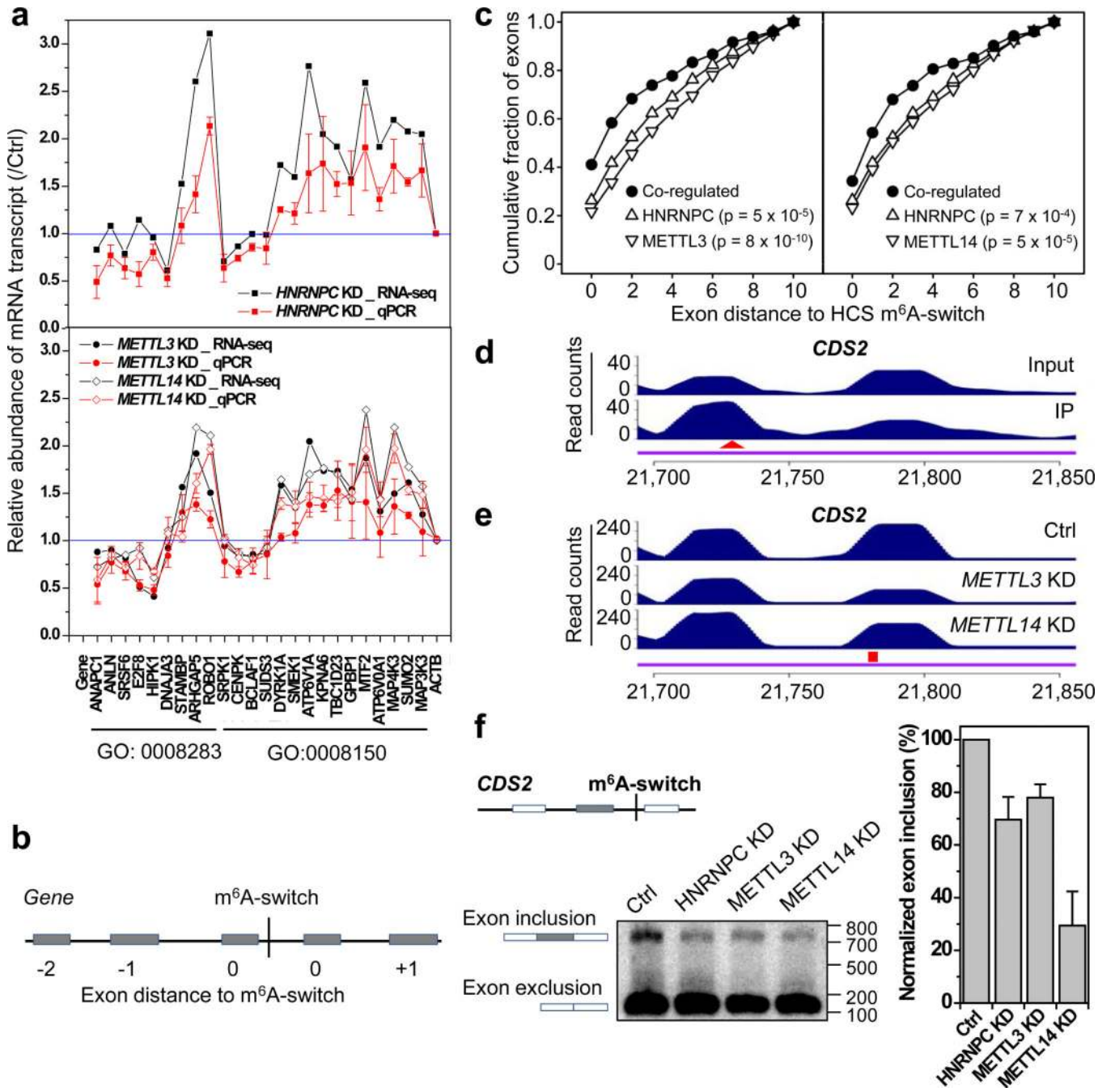

Figure 4. m^{6}A-switches regulate mRNA abundance and alternative splicing

a, *HNRNPC*, *METTL3/L14* KD co-regulated the abundance of m^{6}A-switch-containing transcripts by RNA-seq and qPCR. **b,** Illustration of the relative exon distance to m^{6}A-switches. **c,** Co-regulated exons by *HNRNPC* KD and *METTL3* KD (left) and *METTL14* KD (right) were more enriched around m^{6}A-switch sites than non-co-regulated exons, Kolmogorov-Smirnov test. **d-f,** Validation of the m^{6}A-switch regulated splicing at one exon neighboring the *CDS2* m^{6}A-switch as shown in PARCLIP-MeRIP data (**d**), *METTL3/L14*

KD data (**e**), and RT-PCR results (**f**). The red triangle and square mark the m^6A site and U-tract, respectively. n = 4, ± s.d., biological replicates.